applied sciences

MDPI

Article

Vibration Characteristics and Foundation-Level Response Assessment of Existing Transmission Towers Subjected to Adjacent Railway Tunnel Blasting

Yan Wang *, Yifan Pan and Yicong Qian

School of Architectural Engineering, Zhejiang Sci-Tech University, Hangzhou 310018, China; 2025220803031@mails.zstu.edu.cn (Y.P.); 2025220803033@mails.zstu.edu.cn (Y.Q.)
* Correspondence: an_wangyan@zstu.edu.cn; Tel.:+86-180-571-678-68

Featured Application

The findings provide practical guidance for blast-charge control, vibration monitoring, and foundation safety assessment during tunnel construction adjacent to existing high-voltage transmission towers.

Abstract

Tunnel blasting adjacent to existing transmission towers may induce foundation vibration and transient deformation, affecting the response evaluation of transmission tower foundations. This study investigates the blast-induced response characteristics of three in-service high-voltage transmission towers adjacent to the Langjiafan Railway Tunnel. Field monitoring was conducted at different longitudinal distances to obtain three-component peak particle velocities (PPVs) and dominant frequencies. Site-specific vibration attenuation relationships were established using the Sadovsky empirical model, and a three-dimensional tunnel–rock mass–transmission tower numerical model was developed and validated against field measurements. The results show that the PPVs generally increased as the tunnel face approached the towers, and the vertical component exhibited relatively larger responses under the investigated blasting conditions. The maximum vertical PPVs of Towers No. 1–3 were 0.9563, 1.1253, and 1.5198 cm/s, respectively, corresponding to 38.3%, 45.0%, and 60.8% of the adopted control value of 2.5 cm/s. The dominant frequencies mainly ranged from 20 to 65 Hz in the horizontal directions, while the vertical components exhibited higher-frequency characteristics under certain blasting conditions. The Sadovsky models achieved coefficients of determination of 0.927, 0.923, and 0.903, and the numerical model reproduced the measured vibration attenuation trends with mean relative errors of 12.48–13.22%. The maximum transient differential foundation displacements of Towers No. 1–3 were 0.1064, 0.1947, and 0.1433 mm, respectively. The results indicate that both foundation vibration velocity and transient deformation should be considered when evaluating the response of transmission tower foundations subjected to adjacent tunnel blasting. The findings provide site-specific references for vibration monitoring and blast-induced response control of existing transmission tower foundations under similar underground blasting conditions.

Keywords: tunnel blasting; high-voltage transmission tower; field monitoring; numerical simulation; peak particle velocity; dominant frequency; vibration attenuation; foundation deformation

Check for updates

Academic Editor: Marco Zucca

Received: 6 August 2026
Revised: 12 September 2026
Accepted: 12 September 2026
Published: 15 September 2026

Copyright: © 2026 by the authors. Licensee MDPI, Basel, Switzerland. This article is an open access article distributed under the terms and conditions of the Creative Commons Attribution (CC BY) license.

1. Introduction

With the rapid development of high-speed railway networks in mountainous regions, an increasing number of tunnel projects have been constructed under complex geological and environmental conditions. The drilling and blasting method remains one of the most widely used excavation techniques for mountain tunnels due to its high efficiency and adaptability. However, only part of explosive energy is consumed for rock fragmentation, while the remaining energy propagates through the surrounding rock in the form of stress waves, generating blast-induced vibrations. These vibrations may affect adjacent sensitive structures, including buildings, pipelines, underground facilities, and transmission towers, especially when blasting operations are conducted close to existing infrastructure [1–3].

Blast-induced vibration propagation and its effects on adjacent structures have been extensively investigated. Previous studies have demonstrated that vibration characteristics are mainly influenced by explosive charge, blasting distance, geological conditions, and propagation paths [4]. Peak particle velocity (PPV) is widely adopted as the primary indicator for evaluating blast-induced vibration because it directly reflects vibration intensity and can be conveniently obtained from field measurements. Meanwhile, empirical attenuation models based on scaled distance have been widely applied to predict vibration attenuation characteristics in engineering practice. However, the parameters of these models are highly dependent on geological conditions and blasting environments and therefore require calibration using field monitoring data before practical application [5,6]. Recent field investigations have further demonstrated that blast-induced vibration attenuation is strongly dependent on propagation direction, monitoring location, and site conditions. Wang et al. [7] investigated tunnel-blasting vibration at different source distances and reported distinct attenuation characteristics at different monitoring locations and directions. Wang et al. [8] further compared several empirical prediction equations for tunnel structures and showed that their prediction performance is closely related to site-specific attenuation coefficients. These findings further emphasize the necessity of calibrating empirical attenuation relationships using project-specific monitoring data.

Based on field monitoring and numerical simulation, numerous studies have investigated the influence of tunnel blasting on adjacent structures. Research has mainly focused on conventional structures, including buried pipelines, buildings, underground facilities, and surrounding rock systems. Jiang et al. [5] analyzed the vibration response of adjacent buried pipelines induced by tunnel blasting, while Li et al. [9] investigated the influence of blasting vibration on adjacent buildings through field monitoring and numerical analysis. Dong et al. [10] investigated blasting stress-wave propagation characteristics in jointed rock masses using numerical simulation, while Ma et al. [11] analyzed the disturbance response of underground storage facilities subjected to adjacent tunnel blasting. Guo et al. [12] investigated the influence of tunnel blasting construction on the surrounding environment based on field monitoring and numerical analysis. More recently, Deng et al. [13] analyzed ground-surface vibration signals induced by blasting excavation in fractured rock and found pronounced directional differences in vibration attenuation and frequency-energy distribution. Lu et al. [14] investigated blast-induced vibration near cross passages in deep tunnels and demonstrated that wave reflection, superposition, and P–S wave conversion can produce significant local amplification or attenuation effects. Wang et al. [15] also showed through field monitoring and numerical analysis that vibration propagation and attenuation characteristics vary considerably with structural position and propagation path in closely spaced tunnel systems. These studies have improved the understanding of blast-induced vibration propagation and structural response mechanisms. However, existing research has mainly concentrated on conventional structures, and investigations on high-voltage transmission towers remain relatively limited.

High-voltage transmission towers exhibit distinct structural characteristics compared with conventional structures, including high flexibility, slender members, and strong interaction between tower foundations and surrounding soil. Their vibration responses are influenced not only by external vibration excitation but also by structural dynamic characteristics and foundation conditions. Chen et al. [16] summarized the dynamic response characteristics and vibration control methods of transmission tower-line systems under different external loads. Duan et al. [17] investigated the vibration characteristics of high-voltage towers subjected to adjacent tunnel blasting based on field monitoring and numerical simulation. Wang et al. [18] further analyzed the dynamic response of transmission towers under controlled tunnel blasting using numerical methods. Although these studies provide valuable references for understanding blast-induced responses of transmission towers, several limitations remain. Meanwhile, the recent advances in blast-vibration propagation research indicate that site-specific geological conditions, propagation paths, and structural configurations can substantially modify both vibration amplitude and frequency characteristics [7,8,13–15], which makes direct extrapolation of conclusions from a single monitoring object or site difficult. Most existing studies focus on individual tower cases, while comparative investigations involving multiple towers with different voltage levels under the same tunnel blasting environment are insufficient. In addition, the combined effects of three-component vibration characteristics, dominant frequency variation, site-specific attenuation behavior, and transient foundation deformation require further investigation.

Therefore, this study investigates the blast-induced vibration characteristics of three existing high-voltage transmission towers adjacent to the Langjiafan Tunnel of the Hangzhou–Wenzhou Railway. Two 1000 kV ultra-high-voltage transmission towers and one 500 kV transmission tower were selected as research objects. Field monitoring was conducted to obtain three-directional peak particle velocities and dominant frequencies under different blasting conditions. The site-specific vibration attenuation relationship was established based on the Sadovsky model. Furthermore, a three-dimensional numerical model was developed and validated using monitoring results to analyze transient foundation displacement and differential foundation deformation. The findings provide a reference for vibration control and construction management of mountain tunnel blasting adjacent to existing transmission towers.

2. Engineering Background

2.1. Tunnel Project Overview

This study is based on the Langjiafan Tunnel of the Hangzhou–Wenzhou Railway in Zhejiang Province, China. The main construction mileage of the tunnel is DK91 + 675.19 to DK92 + 143.27, with a total length of 467.2 m. The tunnel was constructed using the drilling and blasting method. The open-cut section adopted the cut-and-cover method, while the underground excavation section adopted different bench excavation methods according to the surrounding rock conditions.

During tunnel excavation, blast-induced stress waves propagate through the surrounding rock and may affect nearby existing structures. In this project, three existing high-voltage transmission towers were located close to the tunnel alignment. Therefore, controlling blasting vibration and evaluating the vibration response of their foundations were important aspects of construction safety management.

2.2. Overview of Adjacent Transmission Towers and Foundations

Three existing transmission towers are distributed on the southeast side of the tunnel alignment and are numbered 1#, 2#, and 3# along the tunnel construction direction. Towers

1# and 2# are 1000 kV cup-shaped ultra-high-voltage (UHV) transmission towers belonging to the Zhebei–Fuzhou UHV AC transmission line, with a height of 91.6 m. Tower 3# is a 500 kV delta-shaped high-voltage transmission tower, with a height of 66.0 m.

The spatial relationship between the tunnel and transmission towers is shown in Figure 1. The minimum spatial distances between the blasting source position corresponding to the tower foundations and the three towers were 50.69 m, 105.36 m, and 45.31 m, respectively. Among them, Tower 3# had the shortest source-to-foundation distance and therefore represented the closest blasting condition.

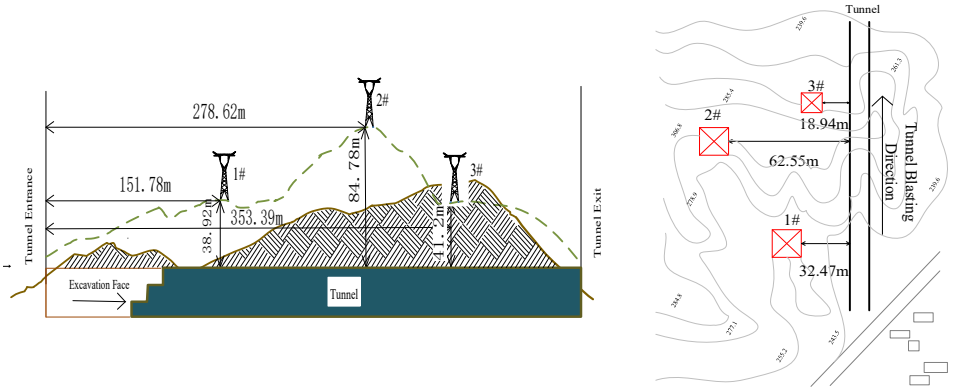


Figure 1. Schematic diagram of tunnel and tower location.

The three transmission towers are supported by independent foundation systems. The foundations are reinforced concrete structures embedded in the surrounding ground. The foundation embedment depths of Towers 1#, 2#, and 3# are approximately 7.9 m, 8.4 m, and 10.8 m, respectively. The main geometric and spatial parameters of the investigated towers and foundations are summarized in Table 1.

Table 1. Spatial and foundation parameters of the investigated transmission towers.

Tower No.	Tower Height (m)	Foundation Type	Root Radius (m)	Foundation Depth (m)	Minimum Horizontal Distance (m)
1#	91.6	Independent foundation	2.05	7.9	32.5
2#	91.6	Independent foundation	1.95	8.4	62.6
3#	66.0	Independent foundation	2.25	10.8	18.9

It should be noted that this study focuses on the vibration response and transient deformation characteristics of tower foundations induced by tunnel blasting. The assessment is based on measured foundation vibration velocity and numerical analysis of foundation response rather than a complete dynamic evaluation of the entire transmission tower system.

The three towers are supported by independent reinforced-concrete foundation systems. According to the available engineering records, the foundation embedment depths of Towers No. 1, No. 2, and No. 3 are approximately 7.9, 8.4, and 10.8 m, respectively, and the corresponding root radii are approximately 2.05, 1.95, and 2.25 m. These geometric parameters, together with the actual spatial positions of the towers relative to the tunnel, were retained in the numerical model to reproduce the principal foundation geometry and source–foundation relationship.

2.3. Engineering Geological Conditions

Grade III, IV, and V surrounding rocks are distributed along the Langjiafan Tunnel alignment. The surrounding rock classification was determined according to the engineer-

ing geological investigation report and the surrounding rock classification criteria adopted in the tunnel design documents.

According to the geological investigation results, the tunnel mainly passes through argillaceous sandstone with different degrees of weathering. The tunnel section beneath the investigated transmission towers mainly consists of Grade III surrounding rock, characterized by weakly weathered argillaceous sandstone with relatively intact rock mass and limited groundwater influence. Local sections containing Grade V surrounding rock were also encountered along the tunnel alignment due to stronger weathering and poorer rock-mass integrity.

The blast vibration propagation characteristics are closely related to the mechanical properties of the surrounding rock. The corresponding physical and mechanical parameters of the Grade III and Grade V surrounding rocks adopted in the numerical model are presented in Section 4.1.

2.4. Blasting Construction Scheme

Emulsion explosives were used during tunnel blasting. The cartridge diameter was 32 mm and the blast-hole diameter was 40 mm. Different excavation methods were adopted according to the surrounding rock grades.

For Grade V surrounding rock, the three-bench temporary invert method was adopted, with a cyclic excavation advance of 0.6 m for the upper bench and 1.0 m for the middle and lower benches.

For Grade III surrounding rock, the upper and lower bench excavation method was adopted, with cyclic advances of 2.0 m and 2.5 m for the upper and lower benches, respectively.

The corresponding blast-hole layouts are shown in Figure 2.

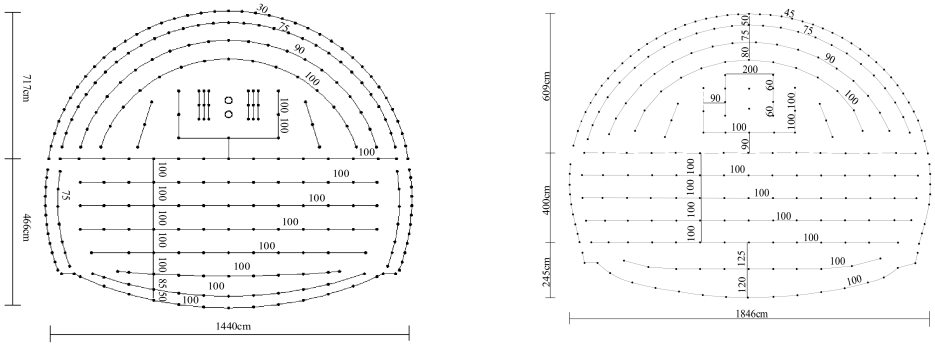


Figure 2. Blast hole layout diagrams. (**a**) Grade V surrounding rock; (**b**) Grade III surrounding rock.

According to the on-site blasting design, the maximum charge per delay refers to the maximum explosive charge initiated within the same millisecond delay interval during one blasting round. The maximum charge per delay was 9.2 kg for the blasting section corresponding to Tower 1#, while 27.6 kg was adopted for the sections corresponding to Towers 2# and 3#.

The difference in charge values resulted from the different blasting designs required for different excavation sections and surrounding rock conditions. These values were determined based on actual construction requirements and were not assigned according to the tower locations.

3. Field Monitoring and Vibration Response Characteristics

3.1. Field Monitoring Scheme

To obtain the actual vibration responses of adjacent high-voltage transmission towers during tunnel blasting, field vibration monitoring was conducted. The investigated

site was located near the construction area of the Hangzhou–Wenzhou high-speed railway tunnel, where blasting operations were carried out close to existing transmission tower foundations.

The monitoring system mainly consisted of three-component vibration sensors and a data acquisition system. As illustrated in Figure 3, monitoring points were arranged at the foundations of three adjacent transmission towers according to the spatial relationship between the blasting source and the monitored towers. The vibration signals induced by blasting were synchronously recorded.

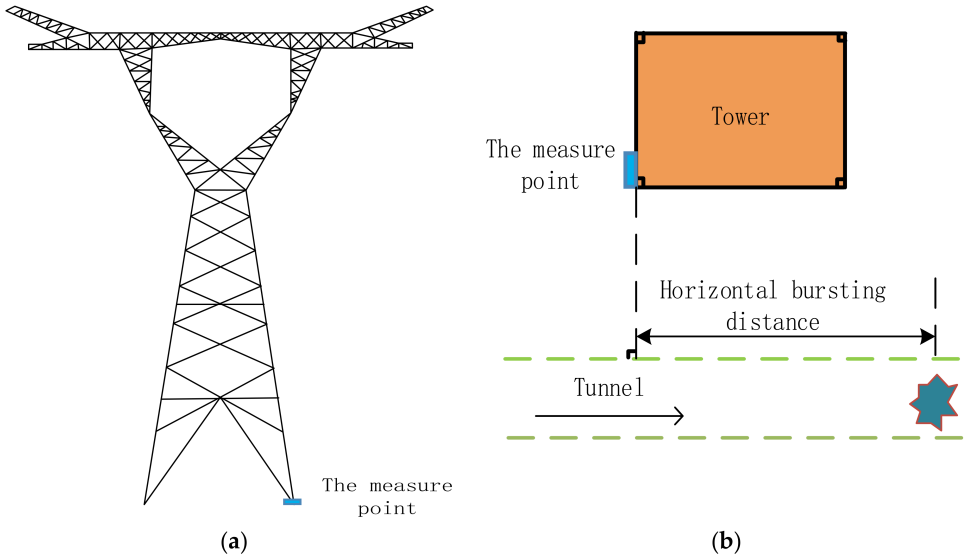


Figure 3. Schematic diagram of vibration monitoring point arrangement. (**a**) Cross-section of tower measurement points. (**b**) Top view of tower measurement point.

The field monitoring process is shown in Figure 4. The vibration sensors were installed on the surface of the tower foundations, and the three-directional vibration velocities, including vertical, radial, and tangential components, were measured.

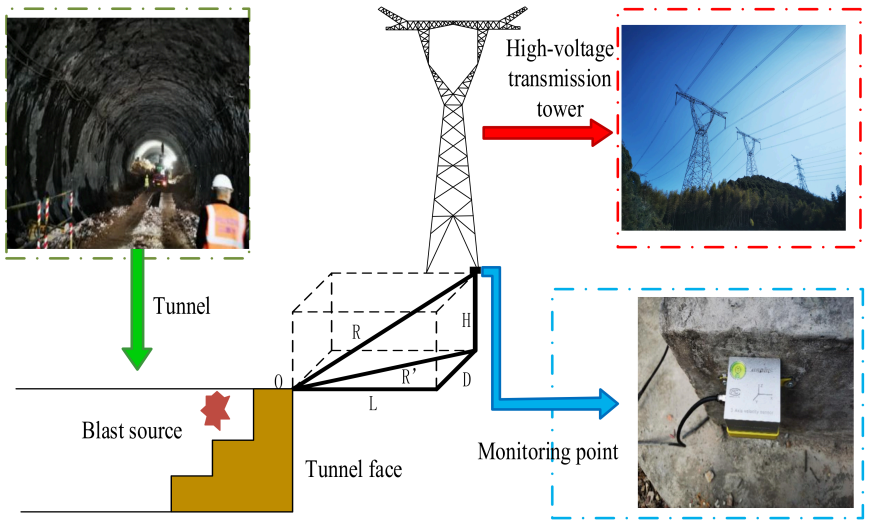


Figure 4. Field vibration monitoring during tunnel blasting construction. Note: L denotes the horizontal blasting distance; R denotes the spatial straight-line distance between the blast source and the monitoring point; R′ denotes the horizontal projected source distance; H denotes the vertical distance; O denotes the reference point of tunnel excavation; D denotes the monitoring point.

The blast-induced vibrations were monitored using an L20-N type blasting vibration monitoring system equipped with three-component velocity sensors. The monitoring system recorded vibration velocities in the vertical, longitudinal, and transverse directions with a sampling frequency of 2000 Hz. The trigger threshold was set as 0.5 mm/s, and the recording duration was 2 s to capture the complete vibration waveform.

The sampling frequency of 2000 Hz was selected to ensure sufficient temporal resolution for capturing the transient characteristics of blast-induced vibration signals. The recording duration of 2 s was adopted to cover the complete waveform evolution, including the vibration onset, peak response, and attenuation stage. The triggering threshold of 0.5 mm/s was selected to capture effective blast-induced vibration signals while avoiding unnecessary recording of background vibrations.

The field measurements were mainly used to obtain foundation-level vibration velocity responses, while the subsequent analysis of transient foundation deformation was conducted through numerical simulation based on the measured vibration characteristics.

During tunnel excavation, the blasting source continuously moved forward, resulting in different relative positions between the blasting face and monitoring towers. Therefore, the horizontal blasting distance L was introduced to describe the relative position between the blasting source and the monitored foundation. The monitoring records corresponding to horizontal blasting distance L of 100, 90, 80, 70, 60, 50, 40, 30, 20, 10, and 0 m were selected for analysis.

It should be noted that L = 0 m only represents the situation when the blasting source reaches the longitudinal position corresponding to the tower foundation. Because the blasting source and foundation still have transverse and vertical offsets, the actual spatial distance between the blasting source and foundation is not zero. Therefore, the spatial source distance R was adopted as the independent variable in the subsequent vibration attenuation analysis.

3.2. Field Monitoring Results

3.2.1. Peak Particle Velocity at the Tower Foundations

The peak particle velocity (PPV) is an important indicator for evaluating blast-induced vibration intensity. The maximum PPV values in the vertical, radial, and tangential directions for the three monitored transmission tower foundations are summarized in Table 2, while the complete distance-dependent monitoring dataset is provided in Supplementary Table S1.

Table 2. Key peak particle velocity indicators for the three transmission tower foundations.

Tower No.	Maximum Charge per Delay, Q (kg)	Minimum Spatial Source Distance, R_{min} (m)	Maximum Radial PPV, $V_{x,max}$ (cm/s)	Maximum Tangential PPV, $V_{y,max}$ (cm/s)	Maximum Vertical PPV, $V_{z,max}$ (cm/s)	Vertical PPV Ratio, A_z	Control-Limit Utilization, η (%)
1	9.2	50.69	0.2170	0.6678	0.9563	5.05	38.3
2	27.6	105.36	0.4463	0.8676	1.1253	4.62	45.0
3	27.6	45.31	0.5289	1.2736	1.5198	5.97	60.8

Note: The maximum PPVs correspond to the condition of L = 0 m. The vertical PPV ratio was calculated as $A_Z = \frac{v_z(L=0m)}{v_z(L=100m)}$, and the control-limit utilization was calculated relative to the adopted project control value of 2.5 cm/s: $\eta = \frac{v_{z,max}}{2.5} \times 100\%$.

The measured results indicate that the vibration response characteristics of different tower foundations varied with blasting conditions and source–receiver distance. The vertical component generally exhibited larger vibration amplitudes than the horizontal

components, which is consistent with the propagation characteristics of blasting-induced stress waves in near-surface environments.

The PPV attenuation characteristics of the three tower foundations are shown in Figure 5. Although Tower 3# had the shortest spatial distance from the tunnel excavation area, the maximum vibration response was not determined solely by source distance. The measured PPV values were influenced by the combined effects of blasting intensity, propagation distance, geological conditions, and local foundation characteristics.

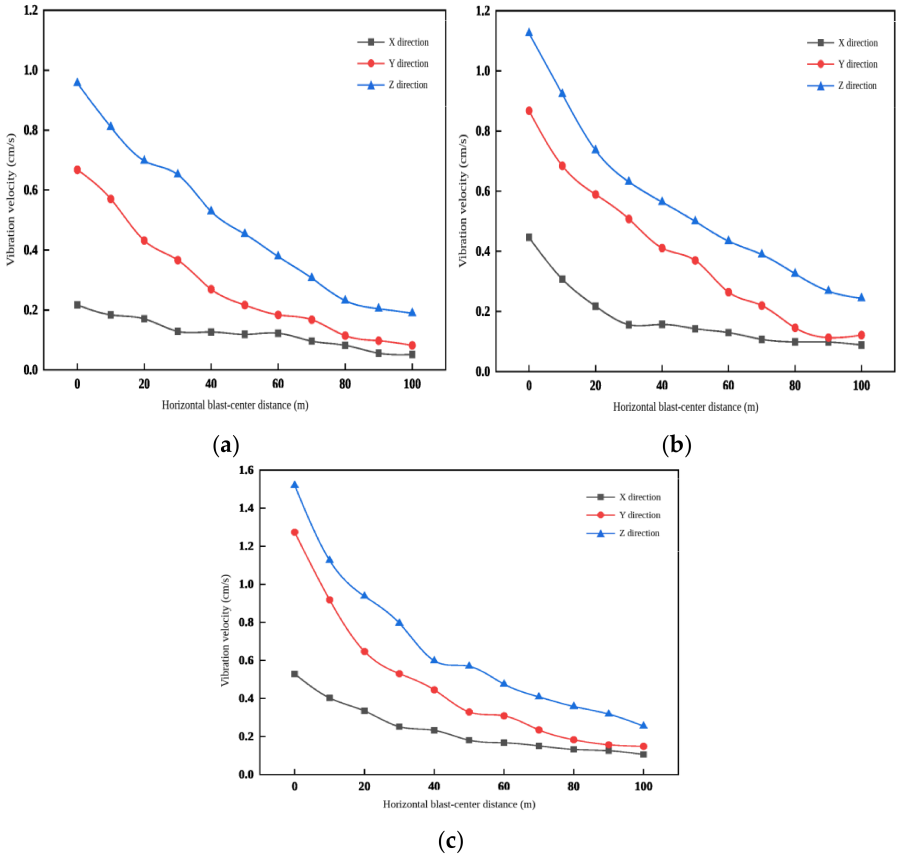


Figure 5. Variations in the measured PPVs with horizontal blasting distance for the three transmission towers. (**a**) Tower No. 1; (**b**) Tower No. 2; (**c**) Tower No. 3.

Figure 5 shows that the tower-foundation PPVs generally increased nonlinearly as the horizontal blasting distance decreased. When the horizontal distance was reduced to approximately 30 m or less, more pronounced increases were observed in several vibration components, indicating that close-range blasting had a greater influence on the tower-foundation vibration responses.

Among the three monitoring directions, the radial PPV was generally the lowest, followed by the tangential component, whereas the vertical PPV was usually the highest. The relatively large vertical response may have resulted from the combined effects of blasting-load characteristics, vibration-wave propagation paths, and local geotechnical conditions surrounding the tower foundations. In the present case, the blasting sources were located inside the tunnel beneath the surrounding ground surface, and the induced stress waves propagated upward through the rock mass toward the tower foundations. This underground-source to surface-foundation propagation path may have enhanced the vertical vibration component compared with the horizontal components. Therefore, the vertical PPV was considered an important indicator for evaluating foundation vibration responses under the investigated blasting conditions.

It should be noted that the absolute vibration responses of the three towers cannot be compared solely on the basis of source distance. The maximum charge per delay was 9.2 kg for Tower No. 1 and 27.6 kg for Towers No. 2 and No. 3. In addition, the propagation distances, rock-mass conditions, and wave propagation paths differed among the towers. Therefore, the observed differences in PPV resulted from the combined effects of explosive charge, source distance, propagation medium, and local site conditions.

According to GB 6722–2014, blast-induced vibration should be evaluated considering both PPV and dominant frequency. For general civil structures, the allowable PPV ranges from 2.0–2.5 cm/s at dominant frequencies of 10–50 Hz and from 2.5–3.0 cm/s above 50 Hz [19]. Although the code does not specify a separate limit for transmission towers, a control value of 2.5 cm/s has been adopted in previous field investigations of high-voltage transmission towers subjected to adjacent tunnel blasting [17]. Considering the measured frequency characteristics and the importance of the in-service transmission facilities, 2.5 cm/s was therefore adopted as the project-specific foundation-level vibration control value in this study. This value is used as an engineering screening criterion for the investigated project rather than as a universal regulatory limit for transmission towers.

3.2.2. Dominant Frequency Characteristics

In addition to PPV, the frequency content of blast-induced vibration is an important factor in evaluating the dynamic response characteristics of transmission towers. When the dominant excitation frequency approaches a structural natural frequency, dynamic amplification may occur. Therefore, the dominant frequencies of the radial, tangential, and vertical vibration signals were extracted. The frequency ranges and mean values obtained from the 11 horizontal blasting-distance conditions are summarized in Table 3, while the complete frequency dataset is provided in Supplementary Table S2.

Table 3. Statistical characteristics of the dominant frequencies measured at the transmission tower foundations.

Tower No.	Monitoring Direction	Dominant Frequency Range (Hz)	Mean Dominant Frequency (Hz)
1	Radial, (X)	34.1–60.2	49.85
1	Tangential, (Y)	23.8–64.0	48.01
1	Vertical, (Z)	44.5–113.8	69.13
2	Radial, (X)	28.4–51.2	40.33
2	Tangential, (Y)	36.6–53.9	46.85
2	Vertical, (Z)	53.9–113.8	76.15
3	Radial, (X)	23.8–44.5	35.66
3	Tangential, (Y)	25.6–46.5	37.14
3	Vertical, (Z)	24.4–68.5	42.56

Note: The mean dominant frequency was calculated from the field monitoring results obtained at 11 horizontal blasting distances for each tower.

As shown in Table 3, the dominant frequencies exhibited a certain degree of scatter among different towers and monitoring directions. Nevertheless, the vertical frequencies were generally higher than the corresponding horizontal components. For Tower No. 1, the mean radial and tangential frequencies were 49.85 and 48.01 Hz, respectively, whereas the mean vertical frequency was 69.13 Hz. Tower No. 2 exhibited the highest mean vertical frequency of 76.15 Hz among all monitored components. Tower No. 3 showed comparatively lower mean frequencies of 35.66, 37.14, and 42.56 Hz in the radial, tangential, and vertical directions, respectively.

The vertical dominant frequencies of Towers No. 1 and No. 2 reached 113.8 Hz and covered substantially broader ranges than their corresponding horizontal components.

Therefore, the measured frequencies should not be simply described as being concentrated within 10–50 Hz. A more accurate interpretation is that the horizontal dominant frequencies were mainly distributed within approximately 20–65 Hz, whereas the vertical components exhibited a broader frequency range and exceeded 100 Hz under some blasting conditions.

The variations in dominant frequency with horizontal blasting distance are presented in Figure 6.

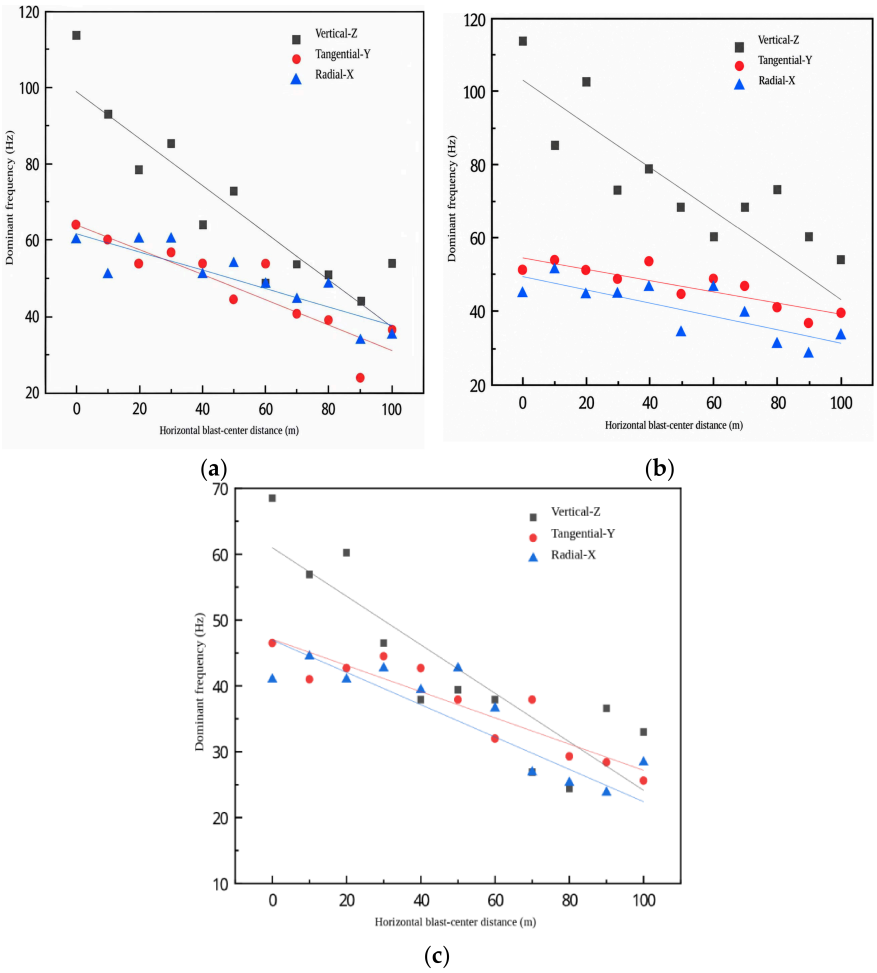


Figure 6. Variations in the dominant frequencies with horizontal blasting distance for the three transmission towers. (**a**) Tower No. 1; (**b**) Tower No. 2; (**c**) Tower No. 3.

Although the measured dominant frequencies fluctuated, the fitted trends generally decreased with increasing horizontal blasting distance. This tendency indicates that high-frequency components may experience stronger attenuation during propagation.

The scatter in the frequency distributions was closely related to the multi-hole and multi-delay characteristics of tunnel blasting. Cut holes, auxiliary holes, perimeter holes, and bottom holes differ in spatial position, charge weight, and initiation sequence. The vibration waves generated by different blastholes are superimposed during propagation, resulting in complex frequency characteristics. In addition, discontinuities, fractures, lithological variations, and local weak zones within the surrounding rock may cause reflection, refraction, scattering, and energy dissipation, thereby broadening the measured frequency distributions.

The measured dominant vibration frequencies reached up to 113.8 Hz. However, because the actual modal properties of the three towers were not obtained in this study, the measured dominant frequencies alone cannot quantitatively evaluate the resonance

relationship between blasting excitation and tower structures. Therefore, the present frequency analysis provides only a preliminary evaluation of the potential dynamic interaction between blast-induced vibration and tower foundations. A more rigorous resonance assessment would require the determination of the actual natural frequencies through ambient vibration testing or validated modal analysis.

According to GB 6722–2014, the allowable blast-induced vibration velocity should be determined by considering both structural type and vibration frequency. Therefore, the frequency characteristics presented in Table 3 and Figure 6 provide an important basis for subsequent safety assessment [19].

3.2.3. Regression Analysis of Blast-Induced Vibration Attenuation

Blast-induced vibration intensity is influenced by the maximum charge per delay, source distance, surrounding-rock properties, and blasting method. To quantitatively describe the variation in tower-foundation PPV with explosive charge and propagation distance under the investigated project conditions, the monitored data were fitted using the Sadovsky empirical equation [20]:

$$v = K\left(\frac{Q^{1/3}}{R}\right)^{\alpha} \quad (1)$$

where v is the maximum tower-foundation PPV in cm/s; Q is the maximum charge per delay in kg; R is the spatial straight-line distance from the blasting source center to the monitoring point in m; K is a site-related coefficient; and α is the vibration attenuation exponent.

The scaled-charge parameter is defined as

$$x = \frac{Q^{1/3}}{R}, \quad (2)$$

and Equation (1) can therefore be rewritten as

$$v = Kx^{\alpha}, \quad (3)$$

The maximum charge per delay adopted in the regression analysis was 9.2 kg for Tower No. 1 and 27.6 kg for Towers No. 2 and No. 3. Nonlinear regression was performed using the scaled-charge parameter x as the independent variable and the maximum tower-foundation PPV as the dependent variable. The fitting results are shown in Figure 7.

The fitted parameters of the Sadovsky attenuation models are summarized in Table 4.

Table 4. Fitted parameters of the blast-induced vibration attenuation models.

Tower No.	Maximum Charge per Delay, Q (kg)	Site Coefficient, K	Attenuation Exponent, α	Coefficient of Determination, R^2
1	9.2	195.28	1.67	0.927
2	27.6	250.43	1.50	0.923
3	27.6	197.89	1.83	0.903

The coefficients of determination for all three towers exceeded 0.90, indicating that the Sadovsky empirical equation reasonably described the overall relationship between the maximum tower-foundation PPV and the scaled-charge parameter under the investigated project conditions.

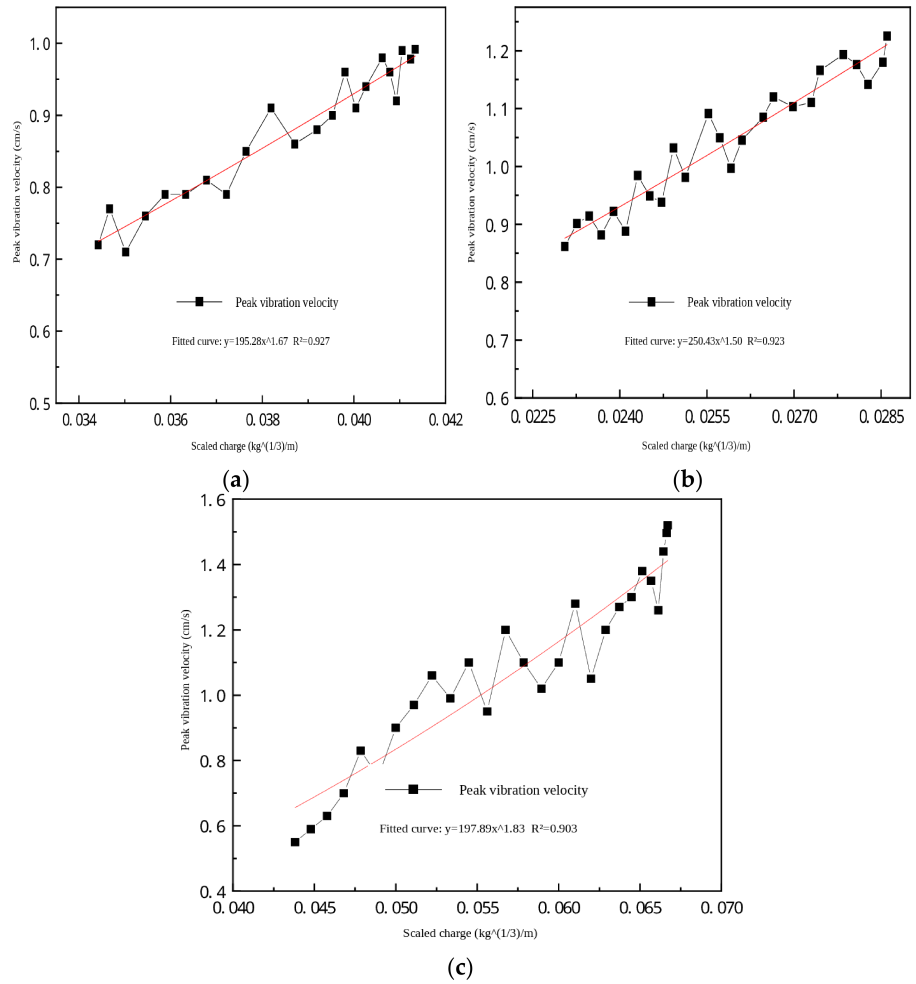


Figure 7. Regression relationships between the maximum PPV and scaled-charge parameter for the three transmission towers. (**a**) Tower No. 1; (**b**) Tower No. 2; (**c**) Tower No. 3.

The fitted attenuation relationships for the three towers are expressed as

$$v_1 = 195.28\left(\frac{Q^{1/3}}{R}\right)^{1.67}, \quad (4)$$

$$v_2 = 250.43\left(\frac{Q^{1/3}}{R}\right)^{1.50}, \quad (5)$$

and

$$v_3 = 197.89\left(\frac{Q^{1/3}}{R}\right)^{1.83}, \quad (6)$$

The attenuation exponents of Towers No. 1, No. 2, and No. 3 were 1.67, 1.50, and 1.83, respectively. Tower No. 3 exhibited the largest attenuation exponent, indicating that its predicted PPV was comparatively sensitive to changes in the scaled-charge parameter. Tower No. 2 had the largest site coefficient K but the smallest attenuation exponent.

The coefficients K and α are affected not only by the surrounding-rock properties but also by blasting parameters, propagation paths, topographic conditions, and monitoring-point locations. Because the three towers differed in maximum charge per delay, spatial position, and wave propagation path, the differences in the fitted parameters should not be attributed solely to the structural characteristics of the towers. The parameters presented in Table 4 should be regarded as site-specific regression coefficients for the geological and

blasting conditions of the present project and should not be directly transferred to other projects without recalibration.

The fitted relationships jointly account for the effects of the maximum charge per delay and spatial source distance and can therefore support project-specific vibration prediction and blasting-parameter control. In Section 5.4, these relationships are inverted to derive preliminary distance-dependent charge-control envelopes. Because the monitoring program primarily covered variations in source distance while the maximum charge per delay remained unchanged within each tower dataset, the inverted charge values are treated as engineering screening estimates rather than independently validated allowable upper limits.

4. Numerical Model Validation and Foundation Response Assessment

4.1. Numerical Model Development

A three-dimensional tunnel–rock mass–transmission tower model was established in MIDAS/GTS to investigate the dynamic response of the adjacent tower foundations during the propagation of blast-induced waves from the tunnel to the ground surface. The model incorporated the entire tunnel alignment, the three transmission towers and their foundations, and the principal topographic features of the site. The overall dimensions were 467 m × 164 m × 122 m. A minimum distance of 40 m was maintained between the tunnel or tower foundations and the external boundaries to reduce the influence of the truncated computational domain on wave propagation.

The rock mass was idealized as a continuous, homogeneous, and isotropic medium governed by the Mohr–Coulomb criterion. Three-dimensional solid elements were used for the tunnel and surrounding rock. In the numerical model, the transmission tower members were represented by Q235 steel beam elements, while the foundations were represented by equivalent C25 concrete pile-type structural elements. The foundation embedment depths and tower-leg layout dimensions were determined from the available engineering records, and the actual relative positions between the tunnel and the three tower foundations were retained. This modeling strategy preserves the main geometric dimensions, material stiffness, mass characteristics, and load-transfer paths governing the foundation-level vibration response.

The equivalent foundation representation was adopted to balance engineering fidelity and computational efficiency. Similar modeling strategies have been used in previous studies of transmission towers subjected to adjacent tunnel blasting, where tower members were modeled using beam elements and foundations using pile elements [17,18]. The model was further validated against field-measured PPVs, showing consistent attenuation trends, $R^2 > 0.93$, and mean relative errors of 12.48–13.22%. These results support the applicability of the equivalent foundation representation for the foundation-level vibration and transient response analysis conducted in this study.

A hybrid mesh was adopted to balance computational efficiency and dynamic-response accuracy, with local refinement around the tunnel excavation boundary, blast-loading region, and tower foundations. Both gravitational loading and blast-induced dynamic loading were included. The numerical model and local mesh are presented in Figure 8.

The material properties and element formulations adopted in the numerical model are summarized in Table 5.

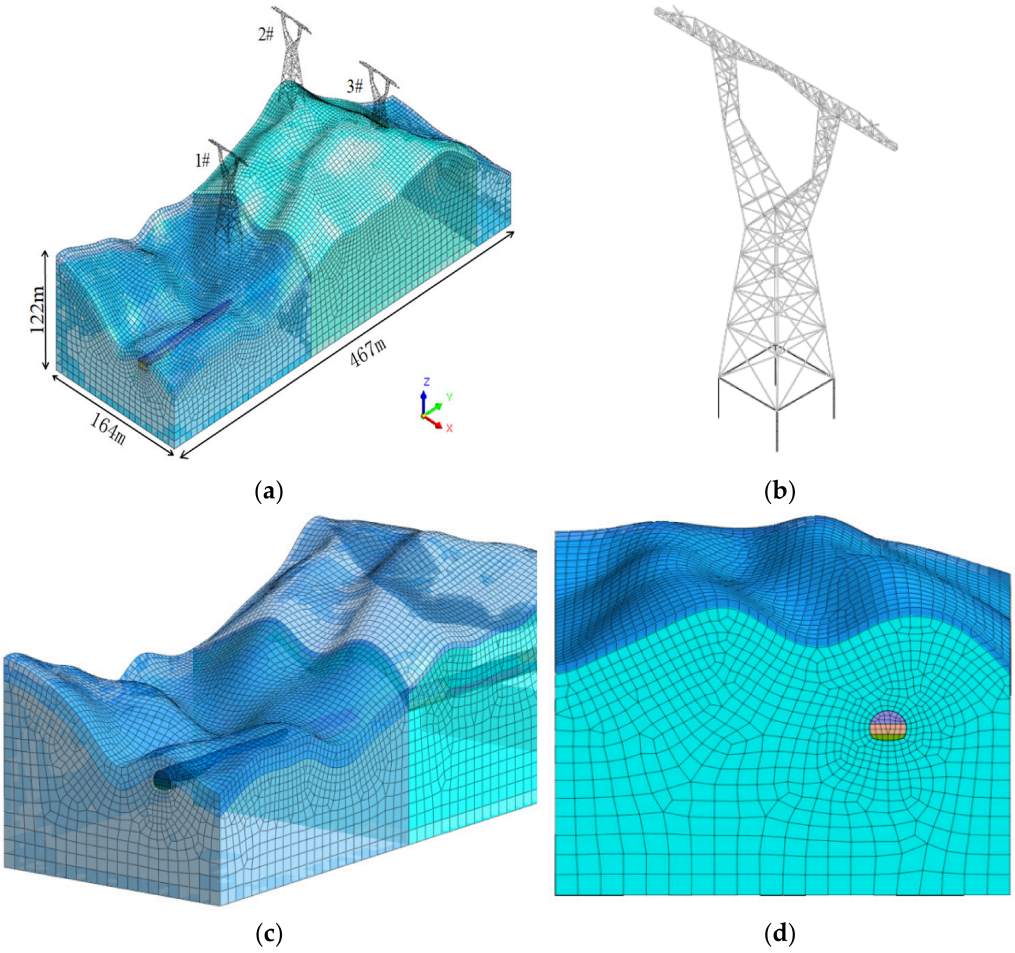


Figure 8. Three-dimensional numerical model of the tunnel–rock mass–transmission tower system. (**a**) Overall computational model; (**b**) transmission tower model; (**c**) local rock-mass model; (**d**) tunnel cross-sectional mesh.

Table 5. Material properties and element formulations adopted in the numerical model.

Material or Component	Rock Grade	Element Type	Constitutive Model	Unit Weight, γ (kN/m^3)	Elastic Modulus, E (GPa)	Poisson's Ratio, ν	Cohesion, c (kPa)	Friction Angle, φ (°)
Strongly weathered sandstone	III	3D solid	Mohr–Coulomb	23.0	11	0.24	200	32
Weakly weathered sandstone	III	3D solid	Mohr–Coulomb	27.2	35	0.17	550	50
Strongly weathered sandstone	V	3D solid	Mohr–Coulomb	22.0	5	0.35	100	25
Weakly weathered sandstone	V	3D solid	Mohr–Coulomb	22.5	13	0.30	200	27
Q235 tower steel	—	Beam	Linear elastic	76.98	206	0.30	—	—
C25 concrete foundation	—	Beam	Linear elastic	25.0	29	0.16	—	—

Artificial reflections may occur when blast-induced stress waves reach the truncated boundaries of a finite model. To reduce their influence on the calculated foundation responses, all translational degrees of freedom were constrained at the bottom boundary, whereas Lysmer–Kuhlemeyer viscous boundaries were assigned to the lateral boundaries [21]. The normal and tangential dashpot coefficients are expressed as

$$C_p = \rho A V_p, C_s = \rho A V_s, \tag{7}$$

where

$$V_p = \sqrt{\frac{\lambda + 2G}{\rho}}, V_s = \sqrt{\frac{G}{\rho}}, \tag{8}$$

and

$$\lambda = \frac{E\nu}{(1+\nu)(1-2\nu)}, G = \frac{E}{2(1+\nu)}. \quad (9)$$

Here, C_p and C_s are the normal and tangential dashpot coefficients, respectively; ρ is the material density; A is the tributary boundary area; V_p and V_s are the P- and S-wave velocities, respectively; and λ and G are the Lamé constant and shear modulus, respectively.

It should be noted that the numerical model was primarily established to evaluate the propagation characteristics of blast-induced vibration and the transient response of tower foundations, rather than to reproduce the complete dynamic behavior of the tower superstructures.

4.2. Equivalent Representation of the Blast Loading

Tunnel blasting involves several types of blastholes, charge configurations, and delay sequences. Explicitly representing each blasthole would substantially increase the computational demand. Therefore, based on Saint-Venant's principle and the equivalent blast-loading method [22], the dynamic action of the blasthole group was represented by a time-dependent pressure applied normal to the tunnel excavation boundary. This treatment was intended to reproduce the overall propagation of blast-induced waves toward the far-field rock mass and tower foundations rather than the near-field rock-fragmentation process. Therefore, the equivalent loading approach was considered appropriate for evaluating the vibration transmission process from the tunnel excavation area to the adjacent tower foundations. The equivalent loading arrangement is illustrated in Figure 9.

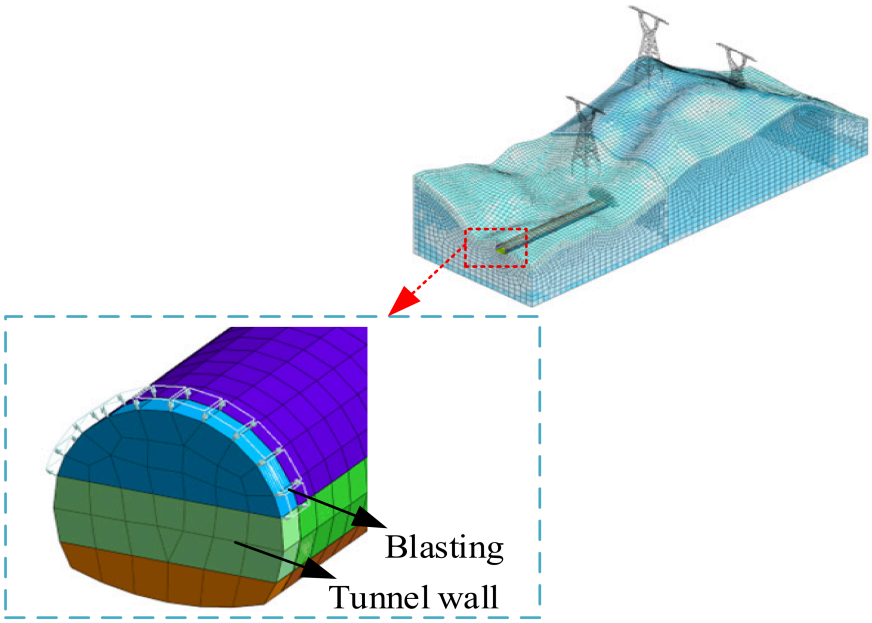


Figure 9. Equivalent blast pressure applied to the tunnel excavation boundary.

The maximum charge per delay adopted in the numerical analyses was consistent with the field blasting scheme. A value of 9.2 kg was used for the tunnel section corresponding to Tower No. 1, whereas 27.6 kg was used for the sections corresponding to Towers No. 2 and No. 3. The principal input parameters for Grades III and V surrounding rock are listed in Table 6.

Table 6. Blast-loading parameters adopted for the two surrounding-rock grades.

Rock Grade	Rock Density (kg/m^3)	P-Wave Velocity (m/s)	Explosive Density (kg/m^3)	Detonation Velocity (m/s)	Equivalent Peak Pressure (MPa)
III	2600	4000	1100	4000	840.5
V	2300	2200	1100	4000	2296

The temporal variation in the equivalent blast pressure was represented using the exponential pressure function proposed by Starfield and Pugliese [23]:

$$P(t) = 4P_b\left[\exp\left(-\frac{Bt}{\sqrt{2}}\right) - \exp\left(-\sqrt{2}Bt\right)\right] \quad (10)$$

where P(t) is the equivalent pressure at time t, P_b is the equivalent peak pressure, and B controls the pressure-decay rate. A value of B = 1000 was adopted. The pressure–time histories used for the different tunnel sections are shown in Figure 10.

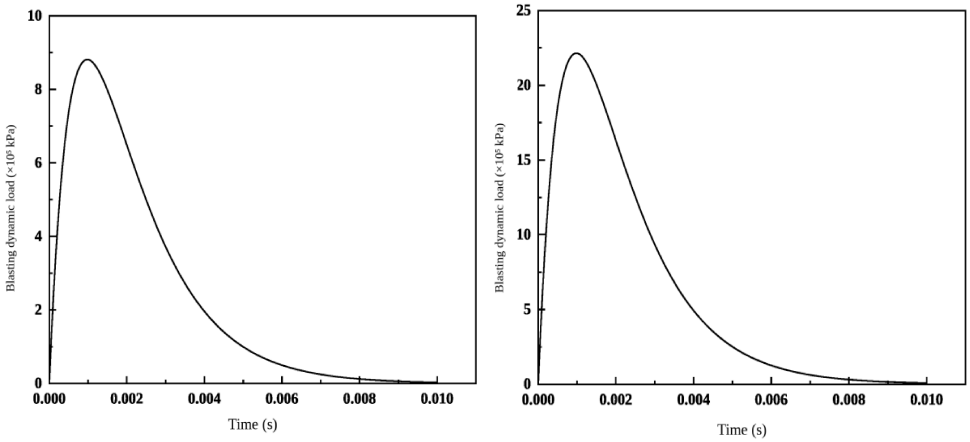


Figure 10. Pressure–time histories adopted in the numerical analyses. (**a**) Tunnel section corresponding to Tower No. 1; (**b**) tunnel sections corresponding to Towers No. 2 and No. 3.

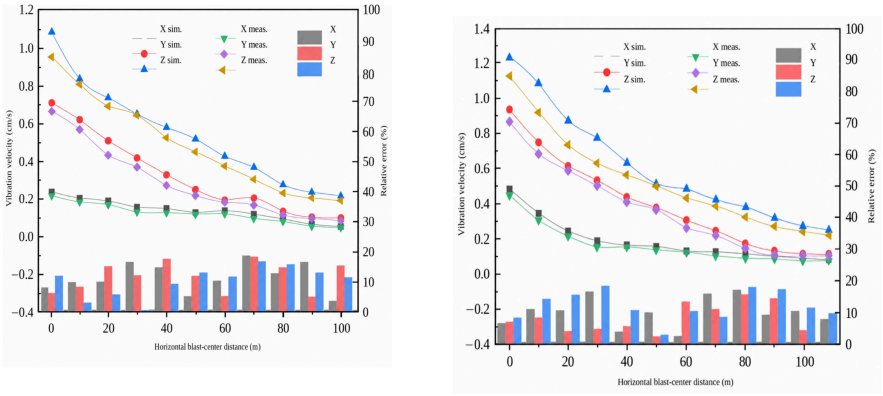
4.3. Validation Against Field Measurements

The numerical model was validated by comparing the simulated and measured PPVs at the three tower foundations. The radial, tangential, and vertical PPVs were extracted for longitudinal blasting distances L of 100, 90, 80, 70, 60, 50, 40, 30, 20, 10, and 0 m. The X-, Y-, and Z-directions corresponded to the radial, tangential, and vertical components, respectively. The complete simulated dataset for the 33 cases is provided in Supplementary Table S3.

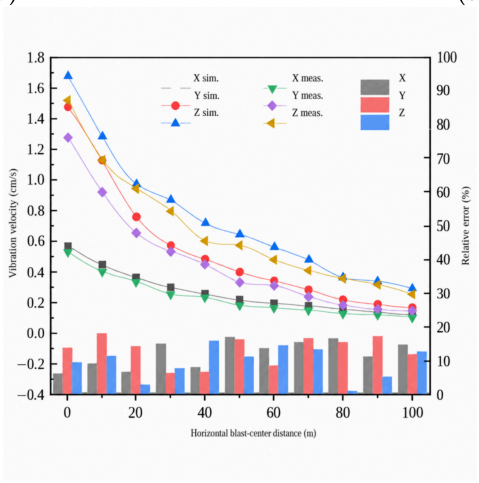
The measured and simulated PPVs are compared in Figure 11.

Both datasets exhibited a consistent distance-dependent trend: the PPVs generally increased as L decreased and reached their maximum values at L = 0 m. The numerical model also reproduced the main response characteristics identified from the field measurements, including the distance-dependent variation in PPV and the relatively larger response of the vertical component under the investigated blasting conditions.

At L = 0 m, the simulated PPVs in the X-, Y-, and Z-directions were 0.2363, 0.7126, and 1.0878 cm/s, respectively, for Tower No. 1; 0.4782, 0.9347, and 1.2311 cm/s for Tower No. 2; and 0.5643, 1.4765, and 1.6788 cm/s for Tower No. 3. The maximum simulated value was the vertical PPV of Tower No. 3, which remained below the project control value of 2.5 cm/s.



(**a**) (**b**)



(**c**)

Figure 11. Comparison between measured and simulated PPVs at the transmission tower foundations. (**a**) Tower No. 1; (**b**) Tower No. 2; (**c**) Tower No. 3.

The statistical validation indices are summarized in Table 7. The coefficients of determination and mean relative errors were calculated using the 33 measured–simulated pairs available for each direction.

Table 7. Statistical validation of the simulated tower-foundation PPVs.

Direction	Maximum Measured PPV (cm/s)	Corresponding Simulated PPV (cm/s)	Critical-Case Relative Error (%)	Coefficient of Determination, (R^2)	Mean Relative Error (%)	Maximum Relative Error (%)
X-direction	0.5289	0.5643	6.7	0.952	13.22	23.47
Y-direction	1.2736	1.4765	15.9	0.943	13.03	23.16
Z-direction	1.5198	1.6788	10.5	0.932	12.48	23.05

The coefficients of determination exceeded 0.93 for all three components, while the mean relative errors ranged from 12.48% to 13.22%. Most individual errors were below 20%, although the maximum error was approximately 23.5%. These results indicate that the model satisfactorily reproduced the overall variation in foundation PPV with the advancing tunnel face.

The simulated PPVs were generally higher than the corresponding measurements, indicating a conservative numerical tendency. This difference was mainly associated with the idealized representation of the rock mass as a continuous, homogeneous, and isotropic medium. In the field, joints, fractures, weak zones, and cavities may cause reflection, scattering, and dissipation of the blast-induced wave energy. In addition, the spatial

arrangement and millisecond-delay sequence of the actual blastholes were represented by an equivalent loading scheme. Despite these simplifications, the validated model captured the distance-dependent attenuation trend and the relative response characteristics among different directions and towers. Therefore, it was further applied to evaluate the transient deformation response of tower foundations under the critical blasting condition.

4.4. Foundation Deformation Under the Critical Blasting Condition

Both the field measurements and numerical simulations identified L = 0 m as the most critical longitudinal position of the blasting source. The vertical displacement histories were therefore extracted at the four individual foundations of each tower under this condition. The foundations were designated as Points A, B, C, and D, as shown in Figure 12.

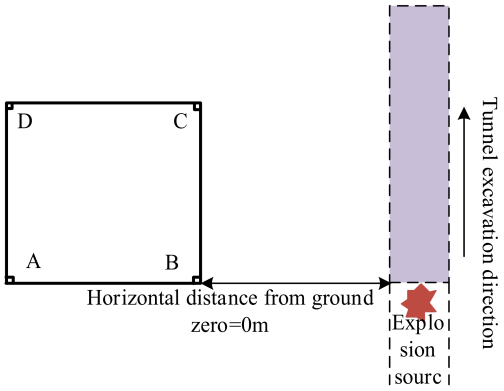


Figure 12. Definition of the four foundation points and their positions relative to the blasting source.

The vertical displacement histories are presented in Figure 13.

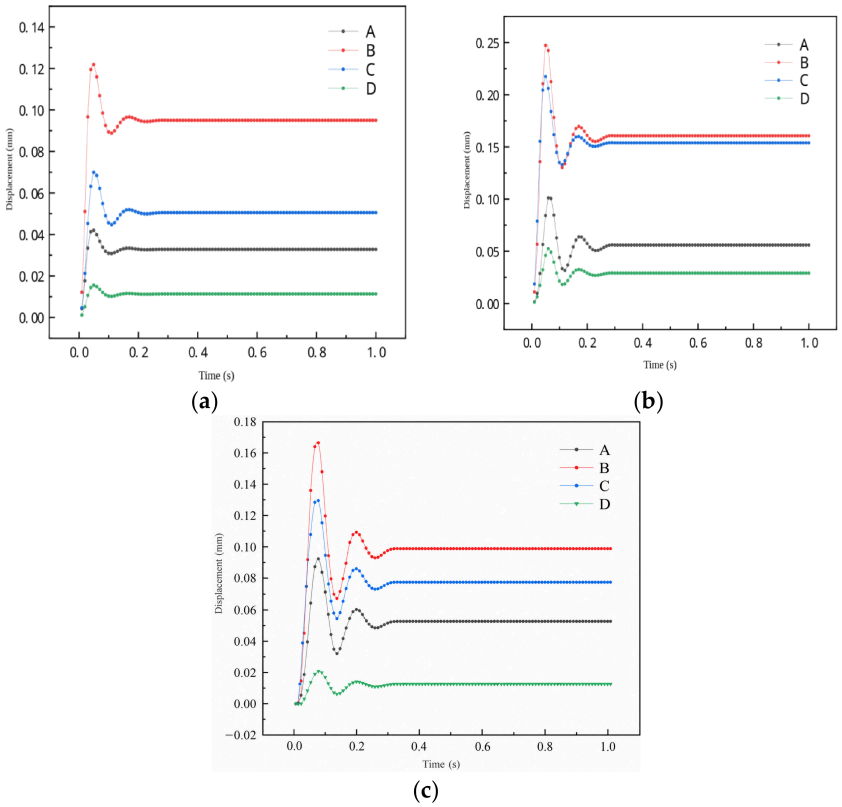


Figure 13. Vertical displacement histories at the four foundation points. (**a**) Tower No. 1; (**b**) Tower No. 2; (**c**) Tower No. 3.

The three towers exhibited similar displacement–time characteristics. The vertical displacements increased rapidly after blast initiation, reached their peak values within approximately 0.05–0.10 s, and subsequently decayed after short-duration oscillations. Point B, which was located relatively close to the blasting source, exhibited the largest response for each tower, whereas Point D consistently showed the smallest displacement. This spatial variation indicates that the blast loading induced nonuniform transient deformation among the four foundations.

The principal vertical-deformation indices are summarized in Table 8.

Table 8. Vertical deformation indices under the critical blasting condition.

Tower No.	Maximum Transient Vertical Displacement (mm)	Maximum Differential Foundation Displacement (mm)	Foundation Inclination Ratio
1	0.1218	0.1064	5.5×10^{-6}
2	0.2471	0.1947	9.5×10^{-6}
3	0.1659	0.1433	1.0×10^{-5}

The differential values in Table 8 represent the maximum transient displacement differences among the four foundation points during blasting and should not be interpreted as permanent post-blast differential settlement. The maximum differential displacement was less than 0.2 mm for all three towers, and the inclination ratios did not exceed 1.0×10^{-5}. According to the reference criteria adopted from JGJ 94–2008 and DL/T 5219–2014 [24,25], the calculated transient deformation indices remained below the corresponding evaluation limits.

Tower No. 3 exhibited the largest foundation PPV, whereas Tower No. 2 developed the largest transient differential foundation displacement. This distinction indicates that vibration velocity and foundation deformation are not governed by exactly the same factors. The PPV is strongly affected by charge weight and source distance, whereas foundation deformation is also influenced by tower configuration, foundation arrangement, structural stiffness, and local ground conditions. Therefore, the safety assessment of transmission towers adjacent to tunnel blasting should consider both foundation PPV and differential foundation deformation rather than relying on a single response indicator.

Under the investigated single-blast conditions, the measured PPVs and calculated transient foundation-deformation indices remained below the evaluation criteria adopted in this study. Tower No. 3 should be prioritized in vibration-velocity monitoring, whereas particular attention should be paid to nonuniform foundation deformation at Tower No. 2.

5. Discussion

5.1. Effects of Source Position on Foundation Vibration

The response increased as the tunnel face approached each tower, but the longitudinal offset L alone does not represent the propagation distance. The spatial distance R, maximum charge per delay, and local propagation path must be considered jointly. Towers No. 2 and No. 3 provide the clearest comparison: both were associated with 27.6 kg per delay, but Tower No. 3 had a much smaller minimum spatial distance and consistently higher PPVs.

The dominance of the vertical PPV was observed for all three towers, suggesting that source geometry and rock–foundation interaction may contribute to the directional response under the investigated blasting conditions. This multi-tower comparison extends previous single-tower studies [17,18,20] and indicates that a single distance measure may not be sufficient for evaluating relative vibration responses among different towers.

Accordingly, near-tower blasting control should be based on a combined charge–distance criterion and should prioritize the vertical component rather than relying only on the tunnel face's plan position.

5.2. Frequency Characteristics and Attenuation Behavior

The horizontal dominant frequencies were mainly 20–65 Hz, whereas the vertical range extended to 113.8 Hz. The overall decrease in dominant frequency with increasing distance is consistent with stronger attenuation of high-frequency content, while the scatter reflects superposition of multiple blasthole groups and spatial variability in the rock mass.

Because the natural frequencies of the towers were not measured, the present frequency data cannot by themselves confirm or exclude resonance. Tower-specific ambient-vibration tests or a validated modal model are required for direct spectral comparison.

The Sadovsky models achieved $R^2 > 0.90$ and provide practical relationships for PPV prediction and preliminary charge-control estimation at this site. Their fitted coefficients combine geological, topographic, blasting, and monitoring effects and therefore require recalibration before use elsewhere.

5.3. Numerical Reliability and Interpretation of the Safety Indicators

The numerical model reproduced the measured distance-dependent PPV variation and the relative response characteristics among different directions. The high coefficients of determination and mean relative errors of approximately 12.5–13.2% indicate that the model can reasonably describe the vibration propagation behavior under the investigated project conditions.

The conservative tendency of the simulated results is physically consistent with the continuous-medium assumption and equivalent blast-loading approach adopted in the numerical model. These simplifications neglect the effects of rock joints, fractures, weak zones, and detailed delay sequences, which may contribute to additional wave attenuation and energy dissipation in field conditions.

The tower exhibiting the largest PPV response was not identical to the tower exhibiting the largest differential foundation displacement. Tower No. 3 showed the largest vibration velocity response, whereas Tower No. 2 exhibited the largest transient differential foundation displacement. This difference suggests that PPV and foundation deformation may be influenced by different factors. Therefore, both vibration velocity and transient foundation deformation should be considered when evaluating the response of transmission tower foundations subjected to adjacent tunnel blasting.

The calculated displacement differences represent transient dynamic responses during blasting and should not be interpreted as permanent post-blast settlement. Long-term deformation behavior requires additional measurements, such as repeated surveying or continuous displacement monitoring after successive blasting events.

5.4. Preliminary Distance-Dependent Charge-Control Envelope

To translate the fitted attenuation relationships into practical construction-control parameters, the Sadovsky equation was inverted to calculate the charge per delay corresponding to a specified PPV threshold:

$$Q_{lim,i}(R) = R^3 \left(\frac{v_{lim}}{K_i} \right)^{3/\alpha_i} \tag{11}$$

where Q_{lim} is the calculated limiting charge per delay for Tower *i*; R is the spatial source distance; v_{lim} is the adopted vibration control value; and K_i and α_i are the tower-specific

regression coefficients listed in Table 4. The adopted project control value of v_{lim} = 2.5 cm/s was used to define the upper charge-control envelope.

For construction management, a warning threshold of 2.0 cm/s, corresponding to 80% of the adopted control value, was introduced to retain a 20% vibration-velocity reserve. The associated management charge was calculated as

$$Q_{w,i}(R) = R^3 \left(\frac{v_w}{K_i} \right)^{3/\alpha_i}, \; v_w = 2.0 \text{ cm/s}, \tag{12}$$

where $Q_{w,i}$ is the charge-control value corresponding to the project-level warning threshold. The value of 2.0 cm/s is introduced in this study as a construction-management threshold rather than as an additional regulatory limit.

For the approximately straight tunnel alignment considered in this study, the spatial source distance at a given longitudinal offset was estimated as

$$R_i(L) = \sqrt{R_{i,min}^2 + L^2}, \tag{13}$$

where $R_{i,min}$ is the minimum spatial source distance at L = 0 m. During actual construction, the surveyed three-dimensional distance between the blasting source and each tower foundation should be used in preference to Equation (13). Representative charge-control values within the near-tower region are summarized in Table 9.

Table 9. Preliminary distance-dependent charge-control envelopes derived from the site-specific attenuation models.

Tower No.	Horizontal Blasting Distance, L (m)	Spatial Source Distance, R (m)	Limiting Charge at 2.5 cm/s, Q_{lim} (kg)	Management Charge at 2.0 cm/s, Q_w (kg)	Field Charge, Q_f (kg)
1	0	50.69	51.8	34.7	9.2
1	20	54.49	64.4	43.1	9.2
1	40	64.57	107.2	71.8	9.2
2	0	105.36	116.6	74.6	27.6
2	20	107.24	122.9	78.7	27.6
2	40	112.70	142.6	91.3	27.6
3	0	45.31	71.8	49.8	27.6
3	20	49.53	93.8	65.1	27.6
3	40	60.44	170.5	118.3	27.6

Note: Q_{lim} was calculated using the adopted project control value of 2.5 cm/s. Q_w was calculated using the project-level warning threshold of 2.0 cm/s. The calculated values represent preliminary site-specific charge-control envelopes and should not be interpreted as authorization to increase the field charge. Any increase beyond the monitored charge range requires additional trial blasting, field verification, and recalibration of the attenuation relationships.

The calculated charge-control values increased with spatial source distance, indicating that the allowable charge estimation at this site should consider the changing spatial relationship between blasting source and tower foundations. At L = 0 m, the management charges corresponding to the warning threshold of 2.0 cm/s were 34.7, 74.6, and 49.8 kg for Towers No. 1–3, respectively, all of which exceeded the field charges adopted in the monitored blasts. Tower No. 3 exhibited the highest utilization of its calculated management envelope and may require relatively greater attention in vibration monitoring under similar conditions. However, because the attenuation models were primarily fitted using measurements obtained at different source distances under fixed charge conditions, the values in Table 9 should be regarded as preliminary screening envelopes rather than

validated allowable upper limits. Any increase beyond the monitored charge range requires trial blasting and field verification.

5.5. Engineering Implications and Limitations

The proposed charge-control envelopes inherit the uncertainties of the field regression models. The rock mass was represented as a continuous medium with uniform material parameters, whereas the actual site contains joints, fractures, weak zones, and local spatial variability. The individual blastholes and their actual millisecond-delay sequence were also represented using an equivalent pressure-loading scheme.

In addition, the monitoring campaign primarily investigated changes in source distance rather than systematic variations in the maximum charge per delay. The charge-control values derived in Section 5.4 therefore require verification through controlled trial blasts before they can be regarded as operational upper limits. Their application should remain within the geological conditions, charge range, and spatial-distance range represented by the present study.

The actual modal properties of the three towers and the long-term post-blast foundation deformation were not measured. Consequently, the present frequency results cannot independently confirm or exclude structural resonance, and the calculated differential displacements should not be interpreted as permanent settlement. Future work should combine ambient-vibration testing, inverse calibration of rock-mass parameters, controlled charge-variation tests, repeated-blast monitoring, and post-blast surveying. Such data would allow the distance-dependent charge-control envelopes to be progressively updated and would support a more comprehensive assessment of cumulative blasting effects.

6. Conclusions

Field monitoring, vibration attenuation regression, and three-dimensional numerical modeling were combined to investigate the effects of railway tunnel blasting on three adjacent high-voltage transmission towers. The principal conclusions are as follows:

1. The measured three-component foundation PPVs generally increased as the tunnel face approached the monitored towers and reached their maximum values at the critical longitudinal position (L = 0 m). Among the three measured components, the vertical PPV was generally dominant under the investigated blasting conditions. The maximum measured vertical PPVs of Towers No. 1–3 were 0.9563, 1.1253, and 1.5198 cm/s, respectively, corresponding to 38.3%, 45.0%, and 60.8% of the adopted project control value of 2.5 cm/s. These results indicate that the vertical vibration response should receive particular attention in foundation-level vibration monitoring for similar underground blasting conditions.
2. The dominant frequency characteristics exhibited directional differences among the three tower foundations. The horizontal dominant frequencies were mainly distributed within approximately 20–65 Hz, while the vertical components showed a wider range and reached up to 113.8 Hz under certain blasting conditions. The dominant frequencies generally decreased with increasing propagation distance. However, because the modal properties of the investigated towers were not measured, the present frequency results cannot independently determine the occurrence of resonance.
3. The Sadovsky attenuation relationships established using field monitoring data achieved coefficients of determination of 0.927, 0.923, and 0.903 for Towers No. 1–3, respectively. The fitted models effectively described the relationship between PPV, charge weight, and spatial source distance under the specific geological and blasting conditions of the investigated site. Their parameters should be recalibrated before application to other engineering projects.

4. The numerical model reproduced the measured distance-dependent PPV variation and the relative response characteristics among different directions and towers. The coefficients of determination exceeded 0.93 for all three components, and the mean relative errors ranged from 12.48% to 13.22%. The simulated responses were generally conservative compared with the field measurements.
5. The numerical analysis indicated that the maximum transient differential foundation displacements of Towers No. 1–3 were 0.1064, 0.1947, and 0.1433 mm, respectively, and the corresponding inclination ratios were below 1.0×10^{-5}. Tower No. 3 exhibited the largest PPV response, whereas Tower No. 2 exhibited the largest transient differential foundation displacement. This difference indicates that vibration velocity and transient deformation may be controlled by different factors, and both indicators should be considered when evaluating the response of tower foundations subjected to adjacent blasting.
6. Based on the site-specific attenuation relationships, preliminary distance-dependent charge-control envelopes were developed for construction reference. At the critical position (L = 0 m), the calculated management charges corresponding to the warning threshold of 2.0 cm/s were 34.7, 74.6, and 49.8 kg for Towers No. 1–3, respectively. Since the monitoring data mainly reflected variations in source distance rather than systematic changes in charge weight, these results should be regarded as preliminary engineering screening values rather than validated allowable charge limits.

Supplementary Materials: The following supporting information can be downloaded at: https://www.mdpi.com/article/10.3390/app16189145/s1, Table S1: Complete field-monitored PPV dataset for the three transmission tower foundations; Table S2: Complete dominant-frequency dataset for the three transmission tower foundations; Table S3: Complete simulated PPV dataset for the three transmission tower foundations.

Author Contributions: Conceptualization, Y.W. and Y.P.; methodology, Y.W. and Y.P.; software, Y.P.; validation, Y.P. and Y.Q.; formal analysis, Y.P.; investigation, Y.P. and Y.Q.; resources, Y.W.; data curation, Y.P.; writing—original draft preparation, Y.P.; writing—review and editing, Y.W. and Y.P.; visualization, Y.P.; supervision, Y.W.; project administration, Y.W.; funding acquisition, Y.W. All authors have read and agreed to the published version of the manuscript.

Funding: This research received no external funding.

Institutional Review Board Statement: Not applicable.

Informed Consent Statement: Not applicable.

Data Availability Statement: The data presented in this study are available within the article and its Supplementary Materials. Additional data are available from the corresponding author upon reasonable request.

Acknowledgments: The authors thank the construction and monitoring personnel for their assistance with the field vibration measurements.

Conflicts of Interest: The authors declare no conflicts of interest.

Abbreviations

The following abbreviations are used in this manuscript:

Abbreviation	Full Term
PPV	Peak particle velocity
UHV	Ultra-high voltage

References

1. Dowding, C.H. *Construction Vibrations*; Prentice Hall: Upper Saddle River, NJ, USA, 1996.
2. Persson, P.A.; Holmberg, R.; Lee, J. *Rock Blasting and Explosives Engineering*; CRC Press: Boca Raton, FL, USA, 1994.
3. Siskind, D.E.; Stagg, M.S.; Kopp, J.W.; Dowding, C.H. *Structure Response and Damage Produced by Ground Vibration from Surface Mine Blasting*; U.S. Bureau of Mines Report of Investigations: Washington, DC, USA, 1980.
4. Singh, P.K.; Roy, M.P. Damage to surface structures due to blast vibration. *Int. J. Rock Mech. Min. Sci.* **2010**, *47*, 949–961. [CrossRef]
5. Jiang, N.; Gao, T.; Zhou, C.; Luo, X. Effect of excavation blasting vibration on adjacent buried gas pipeline in a metro tunnel. *Tunn. Undergr. Space Technol.* **2018**, *81*, 590–601. [CrossRef]
6. Sadovsky, M.A. Mechanical effects of air shock waves from explosions according to observations made in the USSR. In Proceedings of the Second United Nations International Conference on the Peaceful Uses of Atomic Energy, Geneva, Switzerland, 1–13 September 1958.
7. Wang, J.; Ma, B.; Ning, B.; Kou, H.; Li, J. Study on the propagation and attenuation characteristics of tunnel blasting vibration waves at different blast center distances. *J. Appl. Geophys.* **2024**, *220*, 105280. [CrossRef]
8. Wang, X.; Hou, X.; Yuan, W.; He, C.; Sarfarazi, V.; Fan, H. Attenuation of blast-induced vibration on tunnel structures. *Geohazard Mech.* **2024**, *2*, 153–163. [CrossRef]
9. Li, Y.; Luo, L.; Yang, G.; Zhang, L.; Luo, J. Impact of tunnel blasting on the safety of adjacent buildings. *Eng. Blasting* **2022**, *28*, 123–129.
10. Dong, Q.; Li, X.; Jia, Y.; Sun, J. A Numerical Simulation of Blasting Stress Wave Propagation in a Jointed Rock Mass under Initial Stresses. *Appl. Sci.* **2021**, *11*, 7873. [CrossRef]
11. Ma, L.; Lin, F.; Liu, R.; Liu, P.; Xia, G.; Chen, L. Disturbance and control of national strategic gas storage induced by adjacent tunnel blasting. *Front. Earth Sci.* **2022**, *9*, 807073. [CrossRef]
12. Guo, X.; Jiang, A.; Min, Q. Study on the Influence of Blasting Construction of Double-Layer Superimposed Primary Support Arch Cover Method on the Surrounding Environment. *Int. J. Civ. Eng.* **2024**, *22*, 1045–1059. [CrossRef]
13. Deng, Z.; Meng, J.; Deng, Y.; Ni, J.; Ye, D. Analysis of vibration signals near ground surface during blasting excavation of a tunnel in fractured rock. *Sci. Rep.* **2024**, *14*, 21909. [CrossRef] [PubMed]
14. Lu, Y.; He, B.-G.; Li, Q.; Fu, H. Amplification and attenuation mechanisms of blast-induced vibration adjacent to cross passage in deep tunnels. *Transp. Geotech.* **2026**, *56*, 101747. [CrossRef]
15. Wang, X.; Li, J.; Zhao, X.; Liang, Y. Propagation characteristics and prediction of blast-induced vibration on closely spaced rock tunnels. *Tunn. Undergr. Space Technol.* **2022**, *123*, 104416. [CrossRef]
16. Chen, B.; Guo, W.H.; Li, P.Y.; Xie, W.P. Dynamic responses and vibration control of the transmission tower-line system: A state-of-the-art review. *Sci. World J.* **2014**, *2014*, 538457. [CrossRef] [PubMed]
17. Duan, L.; Lin, W.; Lai, J.; Zhang, P.; Luo, Y. Vibration characteristic of high-voltage tower influenced by adjacent tunnel blasting construction. *Shock. Vib.* **2019**, *2019*, 8520564. [CrossRef]
18. Wang, F.; Zhang, G.; Li, W.; Nie, H. Numerical Investigation into the Effects of Controlled Tunnel Blast on Dynamic Responses of the Transmission Tower. *Adv. Civ. Eng.* **2023**, *2023*, 6021465. [CrossRef]
19. *GB 6722-2014*; Safety Regulations for Blasting. Standards Press of China: Beijing, China, 2014.
20. Wu, Y.; Jia, Y.S.; Huang, X.W.; Liu, C.B.; Zhou, X.L.; Xu, H.J.; Liu, F. Analysis of vibration effects of tunnel blasting on adjacent high-voltage transmission towers. *Blasting* **2022**, *39*, 165–171, 198.
21. Lysmer, J.; Kuhlemeyer, R.L. Finite dynamic model for infinite media. *J. Eng. Mech. Div.* **1969**, *95*, 859–877. [CrossRef]
22. Zhang, Y.; Yang, G.; Liu, P.; Yao, J.; Jiang, Y. An equivalent approach for acting blasting load in dynamic numerical simulation of blasting vibration. *Chin. J. Undergr. Space Eng.* **2012**, *8*, 56–64.
23. Starfield, A.M.; Pugliese, J.M. Compression waves generated in rock by cylindrical explosive charges: A comparison between a computer model and field measurements. *Int. J. Rock Mech. Min. Sci. Geomech. Abstr.* **1968**, *5*, 65–77. [CrossRef]
24. *JGJ 94-2008*; Technical Code for Building Pile Foundations. China Architecture & Building Press: Beijing, China, 2008.
25. *DL/T 5219-2014*; Technical Code for Design of Foundation of Overhead Transmission Line. China Planning Press: Beijing, China, 2014.

Disclaimer/Publisher's Note: The statements, opinions and data contained in all publications are solely those of the individual author(s) and contributor(s) and not of MDPI and/or the editor(s). MDPI and/or the editor(s) disclaim responsibility for any injury to people or property resulting from any ideas, methods, instructions or products referred to in the content.